

MORPHOLOGIES OF TWO MASSIVE OLD GALAXIES AT $Z \sim 2.5$ ¹

ALAN STOCKTON² AND ELIZABETH MCGRATH

Institute for Astronomy, University of Hawaii, 2680 Woodlawn Drive, Honolulu, HI 96822

GABRIELA CANALIZO

Department of Physics and Astronomy, University of California, Riverside, CA 95521

MASANORI IYE

Optical and Infrared Astronomy Division, National Astronomical Observatory of Japan, Mitaka, Tokyo, 181-8588, Japan

AND

TOSHINORI MAIHARA

Department of Astronomy, Kyoto University, Kitashirakawa-Oiwake-cho, Sakyo-ku, Kyoto 606-8502, Japan

Draft version February 2, 2008

ABSTRACT

We present the results of NICMOS imaging of two massive galaxies photometrically selected to have old stellar populations at $z \sim 2.5$. Both galaxies are dominated by apparent disks of old stars, although one of them also has a small bulge comprising about 1/3 of the light at rest-frame 4800 Å. The presence of massive disks of old stars at high redshift means that at least some massive galaxies in the early universe have formed directly from the dissipative collapse of a large mass of gas. The stars formed in disks like these may have made significant contributions to the stellar populations of massive spheroids at the present epoch.

Subject headings: galaxies: high-redshift—galaxies: formation—galaxies: evolution

1. INTRODUCTION

Considerable observational evidence has built up over the past few years that a substantial fraction of the massive galaxies around us today were already massive at very early epochs. This evidence comes primarily from three sources:

- Studies of local massive elliptical galaxies indicate that the stars in the most massive galaxies generally formed very early and over very short time intervals (Peebles 2002; Thomas et al. 2005; Nelan et al. 2005; Renzini 2006). Stars in less massive spheroids formed, on average, later and over longer time spans.
- Massive galaxies in clusters show little evidence for significant evolution up to at least redshift ~ 1 (e.g., de Propris et al. 2007; Scarlata et al. 2007).
- Direct observations of massive galaxies at redshifts $\gtrsim 1.5$ that are dominated by already old stellar populations show that significant numbers

of massive galaxies were in place at even earlier epochs (e.g., Stockton, Canalizo, & Maihara 2004; McCarthy et al. 2004; van Dokkum 2004; Labbé et al. 2005; Daddi et al. 2005; Reddy et al. 2006; Papovich et al. 2006; Kriek et al. 2006; Abraham et al. 2007).

Although the existence of massive galaxies at high redshifts is now well documented, there have been only a few high-resolution studies of their morphologies (e.g., Yan & Thompson 2003; Stockton et al. 2004; Zirm et al. 2007; Toft et al. 2007). Morphologies are important, because they may well retain signs of the formation history of the galaxies. This is particularly true for galaxies that show little or no recent star formation, so that we are able to observe relatively clean examples of the stellar population that formed earliest and that comprises the bulk of the mass of the galaxy. In this paper, we present deep *Hubble Space Telescope* (HST) NICMOS imaging of two galaxies with virtually pure old stellar populations at $z \sim 2.5$. In § 2, we briefly recount how these galaxies were selected. In § 3, we describe the observations and reduction procedures. In § 4 and § 5, we analyze model fits to the images to determine morphologies, and in § 6 we discuss the implications of our conclusions. We assume a flat cosmology with $H_0 = 73 \text{ km s}^{-1} \text{ Mpc}^{-1}$ and $\Omega_M = 0.28$.

2. IDENTIFYING GALAXIES WITH OLD STELLAR POPULATIONS AT HIGH REDSHIFTS

Our procedure for selecting galaxies with old stellar populations is described in some detail in Stockton et al. (2004); here we give a brief synopsis. We observe fields of radio sources in certain specific redshift ranges, selecting galaxies with photometric redshifts consistent with

¹ Based in part on observations made with the NASA/ESA Hubble Space Telescope, obtained at the Space Telescope Science Institute, which is operated by the Association of Universities for Research in Astronomy, Inc., under NASA contract NAS 5-26555. These observations are associated with program no. 10418. Additional data were collected at the Subaru Telescope, which is operated by the National Astronomical Observatory of Japan, and at the W. M. Keck Observatory, which is operated as a scientific partnership among the California Institute of Technology, the University of California, and the National Aeronautics and Space Administration. The Observatory was made possible by the financial support of the W. M. Keck Foundation.

² Also at Cerro Tololo Inter-American Observatory, Casilla 603, La Serena, Chile.

that of the radio source. Radio sources generally serve as beacons for some of the more overdense regions in the early universe. Furthermore, the specific redshift ranges selected are chosen to optimize discrimination with standard filter passbands between old stellar populations and highly reddened star-forming galaxies. One of these redshift ranges is $2.3 < z < 2.7$, for which the 4000 Å break, strong in old stellar populations, falls between the J and H bands. We have used the Bruzual & Charlot (2003) (BC03) spectral synthesis models, and, more recently, preliminary versions of the Charlot & Bruzual (2007) (CB07) models, to evaluate and optimize our photometric selection of old stellar populations at various redshifts. The preliminary CB07 models include more realistic prescriptions for thermally pulsing asymptotic-giant-branch stars (Marigo & Girardi 2007; see also Maraston 2005). Although at low redshifts (and for some SEDs at high redshifts) the new models can significantly lower the masses estimated from K -band photometry, at the redshifts we are considering here for nearly pure old stellar populations, the masses (and ages) change hardly at all. The main effect of using the newer models is to reduce the amount of reddening required to obtain a good fit.

If a stellar population were to have an age of 2 Gyr at $z = 2.5$ (corresponding to all of the stars forming at $z = 9$), its observed colors would be $J - K \approx 3.0$ and $J - H \approx 2.1$. We use a photometric sieve procedure to optimize the selection with respect to available observing time, first obtaining relatively short J and K' integrations (typically 5σ at $J = 23$ and $> 10 \sigma$ at $K' = 20$). If any objects with $J - K' \sim 3$ are found, we then obtain H and deeper J imaging. Finally, for fields with objects matching the expected spectral-energy distributions of an old stellar population at the redshift of the radio source, we attempt to obtain deep imaging at shorter wavelengths (usually either R or I) to set constraints on any residual star formation.

Among the galaxies found by this technique are one each in the fields of the radio galaxy 4C 23.56 (Stockton et al. 2004) and the quasar 4C 05.84. We refer to these galaxies as 4C 23.56 ER1 and 4C 05.84 ER1; they are both luminous objects, and they have stellar populations that appear to be overwhelmingly dominated by old stars.

3. OBSERVATIONS AND DATA REDUCTION

3.1. Ground-Based Optical and Near-IR Observations

We obtained most of the near-IR observations (J , H , and K') with the CISCO IR camera (Motohara et al. 2002) on the 8.2 m Subaru Telescope (Iye et al. 2004) in observing runs on 2000 November 8 (UT), 2001 August 5 and 6, and 2002 May 30–June 1. The images have a scale of $0''.105 \text{ pixel}^{-1}$ and a field of $\sim 1'.8$. In addition, we carried out deep R -band imaging of both fields with the Echelle Spectrograph and Imager (ESI; Sheinis et al. 2002) on the Keck II Telescope on 2002 August 7. Both the IR and optical imaging were reduced according to standard procedures using our own IRAF scripts. The calibrations used observations of UKIRT Faint Standards (Hawarden et al. 2001; Leggett et al. 2006) for the IR photometry and Landolt fields (Landolt 1992) for the R -band imaging.

We also observed 4C 23.56 ER1 at K' with the Subaru 36-element curvature-sensing adaptive optics (AO) sys-

tem (Takami et al. 2004) and the Infrared Camera and Spectrograph (IRCS; Kobayashi et al. 2000) on 2002 August 17. These results were reported by Stockton et al. (2004), but we will refer to them again in this paper. We used IRCS without the AO system, but with excellent natural seeing (final images have FWHM of $0''.35$) to obtain a very deep image of the 4C 05.84 field in the K filter on 2004 August 1. Finally, we obtained J -band imaging of the 4C 05.84 field with NIRC2 and the Keck II laser-guide-star adaptive-optics system on 2007 August 21.

3.2. Hubble Space Telescope NICMOS Observations

The NICMOS observations used the NIC2 camera ($0''.075 \text{ pixel}^{-1}$) and the F110W and F160W filters. They were obtained on UT 2005 January 3 (4C 05.84 ER1, F160W, total exposure 5376 s), 2005 January 4 (4C 23.56 ER1, F160W, total exposure 8192 s), 2005 January 8 (4C 05.84 ER1, F110W, total exposure 8448 s), and 2005 May 16 (4C 23.56 ER1, F110W, total exposure 11264 s) as part of *HST* program 10418. After doing a first-pass combination of the images to get a rough idea of the quality of the data, we went back to the *calnica* processed images and corrected these for bias offsets and inverse flatfield effects using the STSDAS *pedsky* task. Most of the F110W images were obtained in orbits impacted by passages through the South Atlantic Anomaly (SAA) and needed special processing. We used the IDL routine *saa_clean.pro* (Bergeron & Dickinson 2003) to generate an image of the persistence from the routinely taken post-SAA dark images and subtract it from the science images. Finally, for these images, *pedsky* was run again to remove any residual bias pedestals.

We then generated a bad-pixel mask from the data quality file, adding an additional mask for the coronagraphic occulter, which produces background that is detected in both filters. Most of the cosmic rays were removed with the contributed IRAF procedure *lacos_im* (van Dokkum 2001). At this point the images from the individual dither positions were combined onto a subsampled grid with the STSDAS *drizzle* task to produce the final image. To choose the optimum *drizzle* parameters for our purposes, we performed a series of tests with artificial PSFs generated by Tiny Tim³. We ended up choosing a drop size of 0.7 and a subsampling factor of 2. The final combined images had FWHM of $0''.133$ for the F160W images and $0''.115$ for the 4C 23.56 ER1 F110W image. We were unfortunately unable to produce a useful image of 4C 05.84 ER1 in the F110W band because of a combination of the object's low surface brightness at that wavelength and residual effects on the detector of the previous SAA passage. The final 3σ surface brightness limits (in the Vega system) were $\mu_{160} \approx 22.3$ and $\mu_{110} \approx 23.3$ for 4C 23.56 ER1, and $\mu_{160} \approx 22.0$ for 4C 05.84 ER1.

The drizzling process inevitably introduces some level of correlation between adjacent pixels. Where we needed to estimate absolute errors (such as for our radial-surface-brightness plots), we made a statistical correction to the error determinations, following the prescriptions of Fruchter & Hook (2002).

Although we obtained images of stars for point-spread-

³ Tiny Tim was written by J. Krist and can be found at <http://www.stsci.edu/software/tinytim/tinytim.html>

function (PSF) determination at the ends of some of the orbits, PSFs modeled from TinyTim were quite consistent with the stellar profiles. Subtracting TinyTim models from the observed stars gave residuals that were less than 1.5% (rms) of the peak over the central FWHM region (and much lower outside this region), with maximum pixel deviations of 3%. The TinyTim profiles also have the advantage that they can be generated on a subsampled grid to minimize interpolation errors in matching the profiles to the undersampled NICMOS2 images. We accordingly used subsampled TinyTim model profiles in our analysis.

4. 4C 23.56 ER1

In the field of the $z = 2.483$ radio galaxy 4C 23.56, our photometric selection procedure picked out a galaxy that had previously been noted as a very red object by Knopp & Chambers (1997). As mentioned above, we have already reported on our Subaru AO/IRCS imaging of 4C 23.56 ER1 (Stockton et al. 2004; there, the galaxy is referred to as 4C 23.56 KC68). The main conclusions of that paper were that (1) the galaxy indeed has a redshift close to that of the radio galaxy, (2) the best fit to the photometry is an old (2–3 Gyr) stellar population with little reddening ($\lesssim 0.2A_V$ of Calzetti et al. 2000 extinction), and that (3) the morphology of this massive, old galaxy looked surprisingly disklike, with a projected axial ratio of 0.3 and a Sérsic index of 1.5. Because the details of the previous observations are available in that paper, and in a brief follow-up report (Stockton & McGrath 2007), we restrict our discussion here to a comparison of the NICMOS imaging with the previous AO imaging.

The NICMOS F110W and F160W images are shown in Fig. 1, along with the best-fit Sérsic models (convolved with the PSF), the residuals from the subtraction of the models from the data, and, again, the best-fit models (but *without* convolution with the PSF). We determine total magnitudes for 4C 23.56 ER1 from the Sérsic models, finding (on the Vega system) $m_{F110W} = 23.39 \pm 0.17$ and $m_{F160W} = 20.82 \pm 0.04$ after correction for Galactic reddening (Schlegel, Finkbeiner, & Davis 1998). The quoted uncertainties include only sky noise and uncertainty in the sky level; they do not include any deviations between the models and the data (which are in any case quite small over the region of good S/N for the data) or other potential systematic effects.

We discuss the F160W image first, since it has a much higher S/N ratio than does the F110W image. Figure 2 shows the radial-surface-brightness profile for the F160W image of 4C 23.56 ER1, along with the best-fit $r^{1/4}$ -law, exponential, and Sérsic profiles, determined using GALFIT (Peng et al. 2002). Among these, the Sérsic profile clearly gives the best fit, as expected, because of the extra degree of freedom in the model. The Sérsic profile has an index $n = 1.52 \pm 0.06$, an effective radius $r_e = 0''.24 \pm 0.01$, and axial ratio $b/a = 0.32$. The uncertainties in n and r_e have been estimated by re-running the models with the sky level set 1σ above and below its median value. From our Subaru AO imaging in the K' band (Stockton et al. 2004), we had obtained $n = 1.49$, $r_e = 0''.22$, $b/a = 0.33$, so the two independent profiles in different bands are in remarkably good agreement. Although the AO imaging had slightly better FWHM, and the two datasets had similar S/N near the center of the galaxy, the NICMOS2

data extends farther in semi-major axis because of its lower sky background. We show a comparison of the two profiles in the region of overlap in Fig. 3. Both the $r^{1/4}$ -law and exponential profiles fit the observed profile poorly. Adding a small ($r_e = 0''.1$), weak (14% of total light) bulge component to an exponential profile with an $r_e = 0''.26$ gives a fit that is as good as that of the Sérsic profile within a semi-major axis of $0''.6$ but somewhat worse beyond this radius.

The F110W image shown in Fig. 1, which samples the morphology shortward of the 4000 Å break (assuming that 4C 23.56 ER1 has the same redshift as 4C 23.56 itself), superficially has an even more “disky” appearance than does the F160W image. This is partly due to the sharper PSF at this wavelength: notice that the best-fit Sérsic models without PSF convolution look much more similar than do the models with PSF convolution. Nevertheless, there may be a detectable difference in morphology in the two bands. The F110W Sérsic model has an index $n = 1.03 \pm 0.10$ (*i.e.*, essentially a pure exponential), an effective radius of $0''.28 \pm 0''.02$, and $b/a = 0.31$. The radial-surface-brightness profile is shown in Fig. 4, along with the best-fit Sérsic model and the F160W Sérsic model (adjusted by a constant magnitude offset to approximately match the F110W points). The observed differences are barely significant, given the uncertainties, but they seem to indicate a small color gradient, such that the outer parts of the galaxy are slightly bluer (at least out to a semi-major axis of $0''.7$, at which point the uncertainty in the sky background level becomes dominant). This cannot be a large effect because of the tight upper limits on the R and I -band magnitudes (see Stockton et al. 2004). Nevertheless, it does suggest a possible slight decrease in mean age and/or mean metallicity of the stellar population as one progresses from the center to the outskirts of the galaxy.

5. 4C 05.84 ER1

4C 05.84 ER1 was found in the field of the $z = 2.323$ quasar 4C 05.84 (Fig. 5). The SED of 4C 05.84 ER1 is shown in Fig. 6, including photometry from our Spitzer IRAC images, which will be discussed elsewhere in more detail in the context of a larger sample of objects. While, for 4C 23.56 ER1, only upper limits at R and I bands have been obtained, for 4C 05.84 ER1 we have detections at $R = 24.6$ and $I = 23.4$, indicating the presence of some younger stars. In attempting to fit the observed SED, we have explored a range of exponentially decreasing star-forming models as well as instantaneous burst models; we have also considered models with metallicities of solar, 0.4 solar, and 2.5 solar.

The formal best-fit model SED is at a redshift of 2.93, substantially higher than that of 4C 05.84 itself. This model has a 0.4-solar-metallicity population with an age of 900 Myr, an exponential time constant of 100 Myr, and a reddening $A_V = 0.06$ mag. If we restrict ourselves to models with redshifts close to that of the quasar, we get a reasonable fit with a solar-metallicity model with a redshift of 2.40, an age of 1.02 Gyrs, an exponential time constant of 200 Myr, and a reddening $A_V = 0.58$ mag. This model fits the I -band and IRAC $5.8 \mu\text{m}$ photometry less well but the IRAC $7.9 \mu\text{m}$ photometry slightly better. Both of these models are shown in Fig. 6. We have no firm grounds for choosing one of these SEDs over

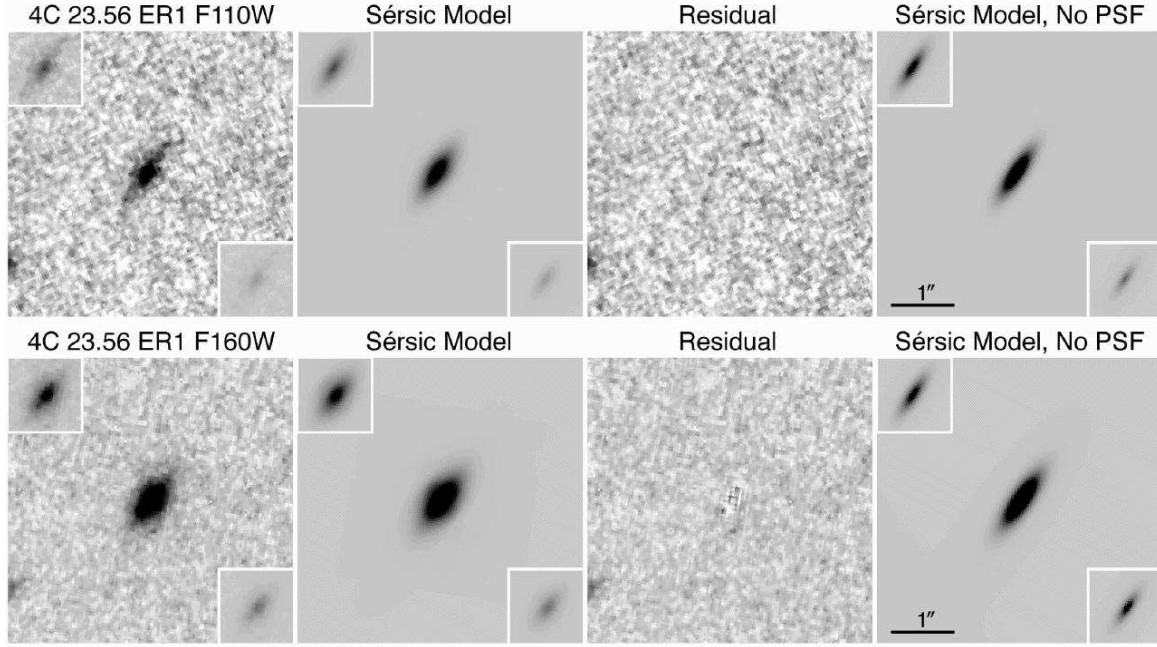


FIG. 1.— NICMOS2 images of 4C 23.56 ER1 in the F110W and F160W filters. The best-fit GALFIT Sérsic models, convolved with the PSF, are shown in the second panel of each row, the difference between the observed images and the models in the third panel, and the models without convolution with the PSF in the last panel. Insets show lower-contrast versions of the images. North is up and East to the left for this and all following images.

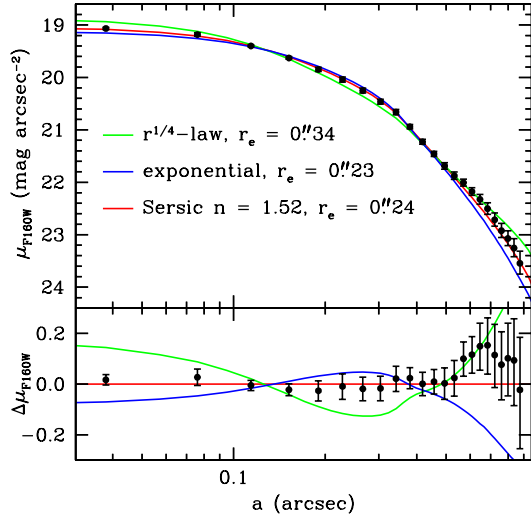


FIG. 2.— Radial-surface-brightness profile of the NICMOS2 F160W image of 4C 23.56 ER1, with best-fit $r^{1/4}$ -law, exponential, and Sérsic profiles shown. The upper panel shows the profiles, and the lower panel shows the deviations of the observed profile and the two other models from the best-fit Sérsic profile. Sample points in this and subsequent plots are at intervals of 1 subsampled pixel in the drizzled images ($0''.038$) along the major axis, so data values and errors for adjacent points are fairly strongly correlated because of drizzling, PSF smearing, and compression of the scale along the minor axis.

the other; but, given the uncertainties in the models and possible star-formation histories, we will accept for the remainder of this paper that the redshift closer to that of 4C 05.84 itself is the correct one. In either case, we are dealing with a massive galaxy comprising stars that mostly formed ~ 1 Gyr before the observed epoch.

We show our NICMOS2 F160W image of 4C 05.84 ER1 in Fig. 7, along with our best-fit GALFIT model. We have

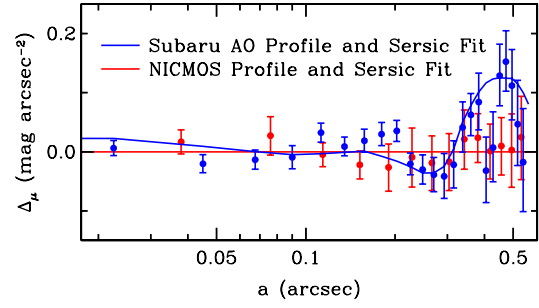


FIG. 3.— Comparison of normalized differential surface-brightness profiles for 4C 23.56 ER1 in the region of overlap. All profiles are shown relative to the NICMOS2 F160W Sérsic fit, and the difference between F160W and K' magnitudes has been removed via a simple slide fit. The red points and line show the F160W profile and Sérsic fit, respectively, and the blue points and line show the Subaru AO K' profile and fit.

tried a series of models, including, again, $r^{1/4}$ -law, exponential, and Sérsic. Radial-surface-brightness profiles of these are shown in the left panel of Fig. 8. In this case, even the Sérsic profile is not a particularly good fit. We get a significantly better fit with a two-component model incorporating a small $r^{1/4}$ -law bulge comprising $31 \pm 15\%$ of the light and an exponential disk accounting for the rest. This model is compared with the best Sérsic profile fit in the right panel of Fig. 8. For the two-component model, the disk component has an effective radius $r_e = 0''.89 \pm 0''.09$, and the bulge component

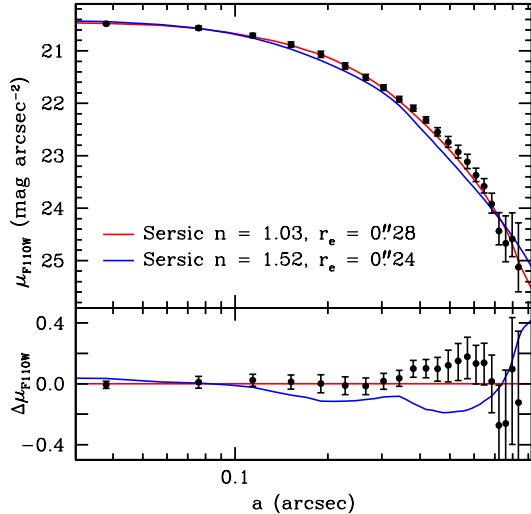


FIG. 4.— Radial-surface-brightness profile of the NICMOS2 F110W image of 4C 23.56 ER1, with best-fit Sérsic profile shown (red trace). Also shown is the best-fit F160W Sérsic profile from Fig. 2, shifted by a constant magnitude offset to match the F110W points (blue trace). The upper panel shows the profiles, and the lower panel shows the deviations of the observed F110W profile and the F160W model from the best-fit Sérsic profile to the F110W data.

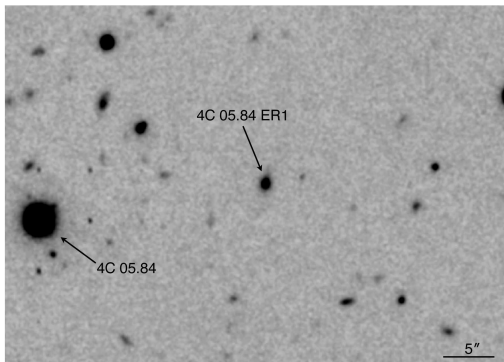


FIG. 5.— The field of 4C 05.84 ER1. The image is a deep (6750 s) K -band integration with the Subaru Infrared Camera and Spectrograph in $0''.35$ seeing. North is up and East to the left.

has $r_e = 0''.37 \pm 0''.2$. This best-fit model gives a total magnitude (on the Vega system) $m_{F160W} = 20.28$.

There is some evidence from our R and I -band imaging and our recent Keck AO imaging in the J band that the bulge component virtually disappears at these shorter wavelengths, indicating that the two morphological components have different stellar populations. Such a result that would not be surprising. The SED shown in Fig. 6 would then be the linear combination of the two SEDs, with the bulge likely being a nearly pure old population and with younger stars being confined to the disk component. We stress, however, that even the disk component must be dominated by old (\sim few hundred Myr) stars, with little very recent star formation. We have experimented with a range of combinations of SEDs at the quasar redshift, but none with simple star-formation histories (instantaneous bursts or exponentially decaying bursts) gave a significantly better fit than did the single-

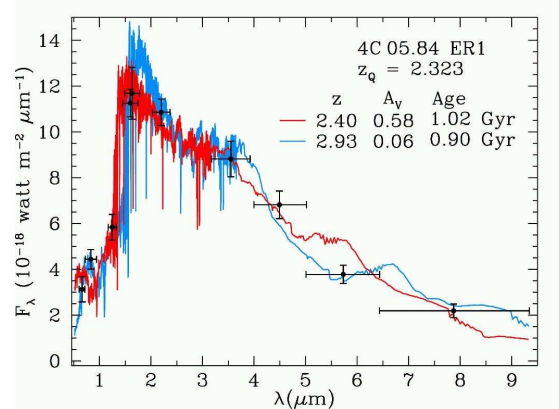


FIG. 6.— Spectral-energy distribution for 4C 05.84 ER1. The blue curve shows the best-fit CB07 stellar population model to the photometry, at a redshift $z = 2.93$. The red curve shows the best-fit model with a redshift close to that of 4C 05.84 itself (z_Q). The redshifts z , Calzetti-law extinctions A_V , and ages of the stellar populations are indicated for each model. See the text for details.

population SEDs shown in Fig. 6. We will explore this possibility in more detail elsewhere.

6. DISCUSSION

Table 1 summarizes the parameters for the two galaxies. The morphologies of both 4C 23.56 ER1 and 4C 05.84 ER1 appear to be dominated by disks of old stars. However, the disks are quite different in scale. 4C 05.84 ER1, at least, also appears to have a small bulge comprising about 1/3 of the total light in the F160W filter ($\sim 4800 \text{ \AA}$, rest frame). We cannot exclude the possibility that 4C 23.56 ER1 also has a weak bulge, with up to $\sim 15\%$ of the total light in the F160W filter; indeed, if the slight apparent difference in morphology between the F160W and F110W images is real, such a difference would seem to favor this possibility.

But it is the presence of massive, old disks that continues to give the strongest constraint on formation mechanisms. Such disks also have been seen at redshifts ~ 1.5 , where normal ellipticals with $r^{1/4}$ -law profiles are also found (Iye et al. 2003; Cimatti et al. 2004; Yan, Thompson, & Soifer 2004; Fu, Stockton, & Liu 2005; Stockton, McGrath, & Canalizo 2006; McGrath et al. 2007). It is difficult to imagine that these massive disks could have formed via any process other than the dissipative collapse of a large cloud of gas. Such disks are also unlikely to have survived major merging events, although the bulge component in 4C 05.84 ER1 may testify to either some level of minor merging activity or bulge building via disk instabilities.

For galaxies at $z \sim 2.5$, the evidence for a dominant old stellar population depends on the inflection in the SED shortward of the H band, and establishing this inflection with optical/near-IR photometry depends on the relatively short baseline from the H to the K band. Furthermore, at the present epoch, essentially all strongly disk-dominated galaxies show evidence for continued star formation. It is therefore not too surprising that claims of passive disks at high redshift should be doubted (e.g., Pierini et al. 2005). However, as Fig. 6 shows, *Spitzer* IRAC data is entirely consistent with the SED of a moderately old stellar population, and no plausible SED incorporating very recent star formation combined with dust would fit the observed pho-

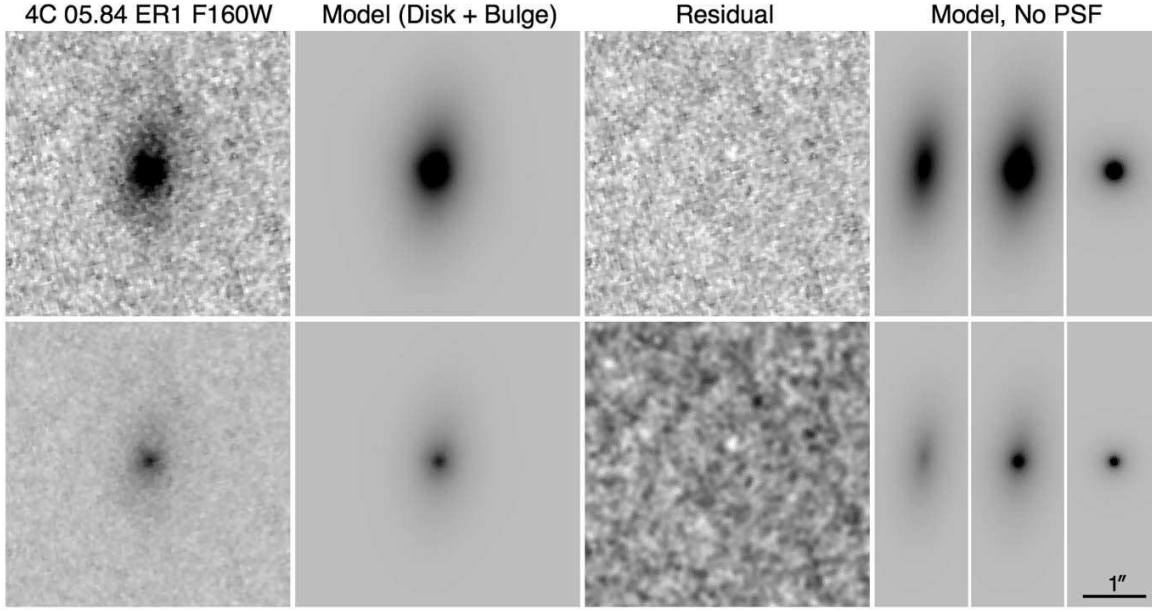


FIG. 7.— The NICMOS2 image of 4C 05.84 ER1 in the F160W filter (left panels). The best-fit GALFIT composite $r^{1/4}$ -law + exponential model, convolved with the PSF, is shown in the second panel of each row, the difference between the observed images and the model in the third panel, and the model without convolution with the PSF in the last panel. This last panel is divided into 3 sub-panels: the middle one of these shows the composite model, the left one shows the exponential component alone, and the right one shows the $r^{1/4}$ -law subcomponent alone. The lower panels show lower-contrast images, except for that for the residual image, which shows a slightly smoothed high-contrast version of the image.

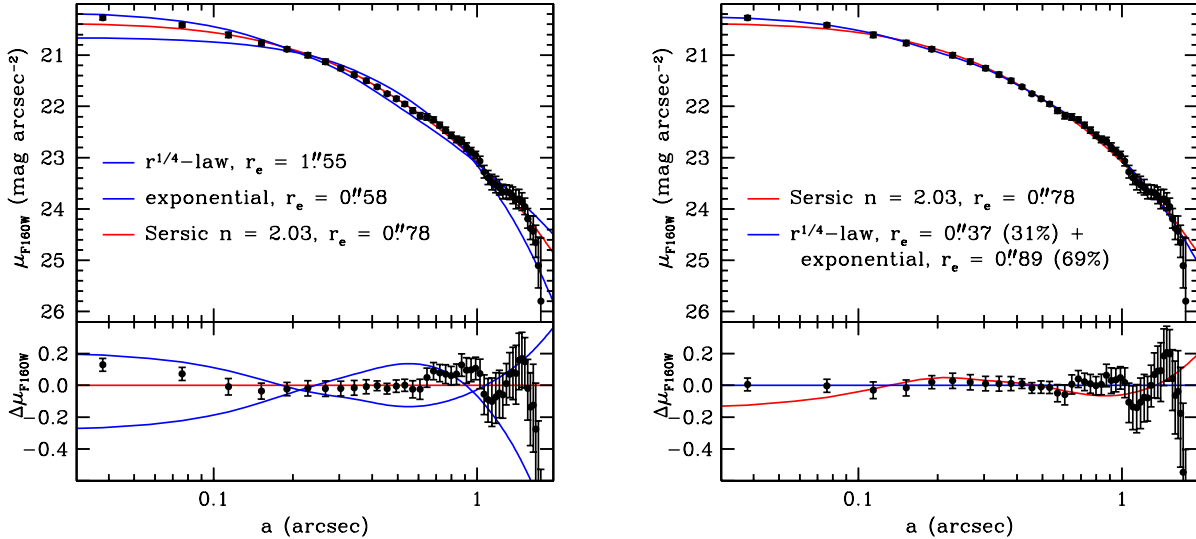


FIG. 8.— Radial-surface-brightness profile of the NICMOS2 F160W image of 4C 05.84 ER1. In the left panel, the best-fit $r^{1/4}$ -law, exponential, and Sérsic profiles are shown in the same way as in Fig. 2. In the right panel, a composite model consisting of a small $r^{1/4}$ -law bulge, accounting for 31% of the light, and an exponential disk comprising the remainder, is compared with the best-fit Sérsic profile. In this case, the differentials in the bottom part of the panel are made with respect to the composite model.

tometry. We have recently also obtained IRAC imaging of the field of 4C 23.56, and our analysis of these data shows that the IRAC photometry falls squarely on our best-fit solar-metallicity BC03 model determined from the optical/near-IR photometry alone: an instantaneous burst with an age of 2.6 Gyr and an extinction $A_V = 0.16$ mag (Stockton & McGrath 2007). Using the more recent preliminary CB07 models, with their improved treatment of AGB stars, we obtain a stellar population age of 2.8 Gyr with $A_V = 0$. Again, no plausible model with signif-

icant star formation and reddening would fit these data.

Masses for these galaxies can be estimated from the model fits. Assuming solar metallicities and a Chabrier (2003) initial mass function, we obtain a mass of $3.9 \times 10^{11} M_\odot$ for 4C 23.56 ER1 and $3.3 \times 10^{11} M_\odot$ for 4C 05.84 ER1 (assuming the model at $z = 2.4$ with $A_V = 0.58$).

While the stellar-population age of 4C 05.84 ER1 indicates that the last major star-formation episode oc-

TABLE 1
MODEL PARAMETERS FOR 4C 23.56 ER1 AND 4C 05.84 ER1

Galaxy	Filter	Sérsic n	r_e ($''$)	r_e (kpc)
4C 23.56 ER1	F110W	1.03 ± 0.10	$0''.28 \pm 0''.02$	2.2 ± 0.2
4C 23.56 ER1	F160W	1.52 ± 0.06	$0''.24 \pm 0''.01$	1.9 ± 0.1
4C 05.84 ER1	F160W	1.00^a	$0''.89 \pm 0''.09$	7.1 ± 0.8
		4.00^a	$0''.37 \pm 0.20$	3.0 ± 1.6

^a The Sérsic indices for the two model components for 4C 05.84 ER1 have been fixed at these values, which correspond to exponential and $r^{1/4}$ -law profiles, respectively.

curred at $z \sim 3.7$, when the universe was ~ 1.8 Gyr old, 4C 23.56 ER1 has a stellar-population age that is formally slightly greater than the age of the universe at $z = 2.483$. Clearly, the likely errors in the age determination and the usual caveats regarding the age-metallicity degeneracy mitigate any implied paradox. Nevertheless, this massive galaxy must have formed at a very high redshift. Models with $[\text{Fe}/\text{H}] = +0.4$ give an age of 1.9 Gyr, but with a significantly worse fit.

It therefore seems likely that galaxy formation models will have to allow for the presence of early-forming massive disks. This means that, at least in some dense regions, it has been possible to form $\sim 3 \times 10^{11} M_\odot$ of stars within a relatively short time via dissipative collapse and without the aid of major mergers. While our selection criteria have ensured that the galaxies we have discussed here comprise essentially pure old stellar populations, they may well be representative of many massive galaxies at high redshift, most of which would not be in our sample if they retained even tiny amounts of residual star formation or if they had had any significant star formation within a few hundred Myr prior to the epoch at which we observe them.

4C 05.84 ER1 has a luminosity and an effective radius that are similar to those of many local galaxies. Our best-fitting Sérsic model has $r_e = 6.3$ kpc. For comparison, for galaxies of similar mass from the Sloan survey with Sérsic $n < 2.5$, Shen et al. (2003) find $r_e = 7.2_{-2.1}^{+2.9}$ kpc. This galaxy could become, with passive evolution and perhaps a few minor mergers to increase the bulge-to-disk ratio somewhat, a typical S0 galaxy at the present

epoch. On the other hand, we do not see galaxies like 4C 23.56 ER1 at the present epoch. By the prescription of Shen et al. (2003), a low-Sérsic-index galaxy with the mass of 4C 23.56 ER1 would have $r_e = 7.6_{-2.2}^{+3.1}$ kpc, but 4C 23.56 ER1 actually has $r_e = 1.9 \pm 0.1$ kpc. This means that the stellar mass surface density is much higher than for local galaxies, a result that has also been found for other samples of distant red galaxies (*e.g.*, Trujillo et al. 2006; Toft et al. 2007). It would seem that the only likely path for such galaxies to evolve to objects consistent with the local population of galaxies is through dissipationless mergers.

There is recent evidence that the most massive galaxies in the local universe are likely the result of dry mergers of galaxies with stars that are already old and with very little gas (*e.g.*, Bernardi et al. 2007). With the constraint that these merging components must themselves mostly be fairly massive (to avoid a large dispersion and flattening in the observed color—magnitude relation for present-day massive galaxies, *e.g.*, Bower, Kodama, & Terlevich 1998), it seems possible that these early massive disks may well be among the sources for the old stars that today are found in the most massive elliptical galaxies.

We thank S. Charlot and G. Bruzual for providing us with preliminary versions of their new spectral synthesis models prior to publication. We also thank the anonymous referee for a detailed reading of the paper and a number of specific suggestions that helped us improve it. Support for *HST* program no. 10418 was provided by NASA through a grant from the Space Telescope Science Institute, which is operated by the Association of Universities for Research in Astronomy, Inc., under NASA contract NAS 5-26555. This research has also been partially supported by NSF grant AST03-07335. It made use of the NASA/IPAC Extragalactic Database (NED) which is operated by the Jet Propulsion Laboratory, California Institute of Technology, under contract with the National Aeronautics and Space Administration.

REFERENCES

- Abraham, R. G. et al. 2007, ApJ, submitted [astro-ph/0701779]
 Bergeron, L. E., & Dickinson, M. 2003, NICMOS Instrument Science Report 2003-010 [http://www.stsci.edu/hst/nicmos/documents/isrs/isr_2003-10.pdf]
 Bernardi, M., Hyde, J. B., Sheth, R. K., Miller, C. J., & Nichol, R. C. 2007, AJ, 133, 1741
 Bower, G., Kodama, T., & Terlevich, A. 1998, MNRAS, 299, 1193
 Bruzual, G., & Charlot, S. 2003, MNRAS, 344, 1000
 Calzetti, D., Armus, L., Bohlin, R. C., Kinney, A. L., Kornneef, J., & Storchi-Bergmann, T. 2000, ApJ, 533, 682
 Cimatti, A., et al. 2004, Nature, 430, 184
 Chabrier, G. 2003, PASP, 115, 763
 Charlot, S., & Bruzual, G. 2007, in preparation
 Daddi, E., et al. 2005, ApJ, 626, 680
 De Propris, R., Stanford, S. A., Eisenhardt, P. R., Holden, B., & Rosati, P. 2007, AJ, in press [astro-ph/0702050]
 Fruchter, A. S., & Hook, R. N. 2002, PASP, 114, 144
 Fu, H., Stockton, A., & Liu, M. 2005, ApJ, 632, 831
 Hawarden, T. G., Leggett, S. K., Letawsky, M. B., Ballantyne, D. R., & Casali, M. M. 2001, MNRAS, 325, 563
 Iye, M. et al. 2004, PASJ, 56, 381
 Iye, M. et al. 2003, ApJ, 590, 770
 Knopp, G. P., & Chambers, K. C. 1996, ApJS, 109, 367
 Kobayashi, N., et al. 2000, in Proc. SPIE 4008: Optical and IR Telescope Instrumentation and Detectors, ed. M. Iye & A. F. Moorwood, p. 1056
 Kriek, M., et al. 2006, ApJ, 649, L71
 Labbé, I. et al. 2005, ApJ, 624, L81
 Landolt, A. U. 1992, AJ, 104, 340
 Leggett, S. K. et al. 2006, MNRAS, 373, 781
 McCarthy, P. et al. 2004, ApJ, 614, L9
 McGrath, E. J., Stockton, A., Canalzio, G., Iye, M., & Maihara, T. 2007, ApJ, submitted
 Maraston, C. 2005, MNRAS, 362, 799
 Marigo, P., & Girardi, L. 2007, A&A, 469, 239
 Motohara, K., et al. 2002, PASJ, 54, 315
 Nelan, J. E., Smith, R. J., Hudson, M. J., Wegner, G. A., Lucey, J. R., Moore, S. A. W., Quinney, S. J., & Suntzeff, N. B. 2005, ApJ, 632, 137
 Papovich, C. et al. 2006, ApJ, 640, 92
 Peebles, P. J. E. 2002, ASP Conf. Ser., 283, 351

- Peng, C. Y., Ho, L. C., Impey, C. D., & Rix, H.-W. 2002, *AJ*, 124, 266
- Pierini, D., Maraston, C., Gordon, K. D., & Witt, A. N. 2005, *MNRAS*, 363, 131
- Reddy, N. A., Steidel, C. C., Fadda, D., Yan, L., Pettini, M., Shapley, A. E., Erb, D. K., & Adelberger, K. L. 2006, *ApJ*, 644, 792
- Renzini, A. 2006, *ARA&A*, 44, 141
- Scarlata, C. et al. 2007, *ApJ*, in press [astro-ph/0701746]
- Schlegel, D. J., Finkbeiner, D. P., & Davis, M. 1998, *ApJ*, 500, 525
- Sheinis, A. I., Bolte, M., Epps, H. W., Kibrick, R. I., Miller, J. S., Radovan, M. V., Bigelow, B. C., & Sutin, B. M. 2002, *PASP*, 114, 851
- Shen, S., Mo, H. J., White, S. D. M., Blanton, M. R., Kauffmann, G., Voges, W., Brinkmann, J., & Csabai, I. 2003, *MNRAS*, 343, 978
- Stockton, A., Canalizo, G., & Maihara, T. 2004, *ApJ*, 605, 37
- Stockton, A., & McGrath, E. 2007, *ASP Conf Ser*, in press [astro-ph/0702130]
- Stockton, A., McGrath, E., & Canalizo, G. 2006, *ApJ*, 650, 706
- Takami, H., et al. 2004, *PASJ*, 56, 225
- Thomas, D., Maraston, C., Bender, R., & Mendez de Oliveira, C. 2005, *ApJ*, 621, 673
- Toft, S., et al. 2007, *ApJ*, in press [arXiv:0707.4484]
- Trujillo, I. et al. 2006, *ApJ*, 650, 18
- van Dokkum, P. G. 2001, *PASP*, 113, 1420
- van Dokkum, P. G., et al. 2004, *ApJ*, 611, 703
- Yan, L., & Thompson, D. 2003, *ApJ*, 586, 765
- Yan, L., Thompson, D., & Soifer, B. T. 2004, *AJ*, 127, 1274
- Zirm, A. W., et al. 2007, *ApJ*, 656, 66